Technical note: „U-Th Analysis" – an open-source software dedicated to MCICPMS U-series-data treatment and evaluation

Inga Kristina Kerber[1], Fabian Kontor[1], Aaron Mielke[1,2], Sophie Warken[1,2], Norbert Frank[1] *

[1] Institute for Environmental Physics, Heidelberg University, Heidelberg, Germany
[2] Institute for Earth Sciences, Heidelberg University, Heidelberg, Germany

Correspondence to: Norbert Frank (mailto:norbert.frank@iup.uni-heidelberg.de)

Abstract

We present our standalone data analysis application for ^{230}Th/U dating on multi-collector inductively coupled plasma mass spectrometers (MC-ICP-MS). The Python-based algorithm is equipped with a graphical user interface (GUI) and comprises raw data treatment, corrections, age calculation, and error estimation. Our underlying measurement protocol employs a combination of Faraday cups (FC) and secondary electron multipliers (SEM), and the software allows for different detector layouts for the measurement of the least abundant isotopes ^{234}U, ^{230}Th and ^{229}Th. We especially focus on features that ensure reproducibility and enable user-friendly reanalysis of measurements such as customized calculation constants with templates. Result files are saved automatically and contain all relevant settings used. Eventually, we demonstrate the relevance of adequate data outlier treatment and generally recommend using the median instead of the mean of calculated ratios. The performance of our evaluation software is demonstrated by a case study from a Puerto Rican stalagmite with growth phases from modern to 40 ka old. The majority of the obtained ages reaches uncertainties in the range of 0.3-0.6%, underlining the capability of our measurement protocol.

1 Introduction

The U-series disequilibrium method, ^{230}Th/U dating, is a precise chronometer covering approximately the last 650 kiloyears, and has proven indispensable for the age determination of marine and continental carbonate archives and their applications (Bourdon et al., 2003). The method is based on a complete disequilibrium of ^{234}U, with its daughter nuclide ^{230}Th, during the formation of secondary carbonates. It presumes a subsequent closed system evolution of the activity ratio of (^{230}Th/^{234}U) and (^{234}U/^{238}U) since the time of formation. Ideally, the initial ^{230}Th activity of the material is presumed zero or can be estimated from the total Th concentration via an initial (^{230}Th/^{232}Th) activity ratio. The dating applications for secondary carbonates and other appropriate materials are manyfold in geochemistry, archaeology, and climate science. Further development of this dating method includes both improvements in instrumentation and measurement protocols, as well as reproducible data analysis and age calculation schemes (Pourmand et al., 2014; Andersen et al., 2004; Cheng et al., 2013; Breton et al., 2015; Chiang et al., 2019; Hellstrom, 2003; Hoffmann et al., 2007; Shen et al., 2002; Shen et al., 2012; Kerber et al., 2023; Shao et al., 2019). The presently most sensitive and precise technology for high precision U and Th isotope measurements is multi-collector inductively coupled plasma source mass spectrometry (MC-ICPMS). Recent technological advances of MC-ICP-MS include the implementation of high ohmic amplifiers allowing to enhance

the dynamic range of multiple Faraday-collectors (FC) to six orders of magnitude for the simultaneous detection of very large and low isotope abundances , instead of the conventionally used combination of secondary electron multipliers (SEM) and FC (Breton et al., 2015). Measurement protocol updates aim at increasing measurement precision and/or decreasing input sample masses by combining new detector layouts, improving the understanding of correction factors, and ensuring a stable measurement environment (Cheng et al., 2013; Chiang et al., 2019; Shen et al., 2002; Shen et al., 2012; Hellstrom, 2003; Andersen et al., 2004; Hoffmann et al., 2007; Kerber et al., 2023; Shao et al., 2019).

We here focus on the third route for the enhancement of ^{230}Th/U dating, which is clear and reproducible data analysis and age calculation schemes. Up to now, only two ^{230}Th/U dating data analysis routines have been published (Shao et al., 2019; Pourmand et al., 2014). However, regarding the rising amount of data being produced in MC-ICP-MS laboratories, data management is becoming more and more important. For example, some samples might require later adaptation of the individual corrections of isotope ratios due to residual contamination with non-carbonate material or detection of initial ^{230}Th from the carbonate forming environment.

Dating young materials of only a few years to centuries in age is challenging due to the small number of counts on especially ^{230}Th, which implies that all correction factors including "ghost signal" corrections need to be determined very precisely (Zhao et al., 2009; Chiang et al., 2019; Kerber et al., 2023). Regarding the removal of scatter ions on the specific low abundance masses 230 and 229 amu, Kerber et al. (2023) demonstrated an effective correction based on a linear dependence of the scattered ions on the ^{238}U signal. Other authors separate U and Th chemically to reduce or remove the ^{238}U beam from the low abundance Thorium isotope measurements (Chiang et al., 2019), which implies flexibility in the detector arrangement and data treatment protocol. As such scatter peaks may depend on the specific instrument or vary through time, these corrections need to be adaptable constants in the data evaluation routine. The influence on final atomic ratio and accuracy of the ghost signals as well as by typical variation in other individual corrections such as peak tailing, mass fractionation, isobaric interferences are evaluated in detail in Kerber et al. (2023).

In addition, the correction for initial Th may cause large age corrections and propagated uncertainties, in particular since adequate initial Th values based on the ^{230}Th/^{232}Th ratio may be variable and difficult to detect (Hellstrom, 2006; Wenz et al., 2016; Wortham et al., 2022). There are different methods to estimate the initial Th isotope ratio: First, isochrons can be used to determine the isotopic composition of the detrital component in the carbonate (Ludwig and Titterington, 1994; Wenz et al., 2016; Stinnesbeck et al., 2020; Töchterle et al., 2022). Secondly, analyses of modern drip waters or recent carbonate deposits allow estimation of the value and sources of initial Th (Wortham et al., 2022; Li et al., 2022). In some cases the "true" age of a stalagmite can be also inferred from other dating methods, such as radiocarbon (Akers et al., 2019; Huang et al., 2024) or the stratigraphic order (Hellstrom, 2006). Also, several approaches can be combined (Warken et al., 2020; Akers et al., 2016; Roy-Barman and Pons-Branchu, 2016).

Other aspects are updating half-lives (such as e. g. from Cheng et al. (2000b) to Cheng et al. (2013)), which makes re-evaluation of previously measured data necessary. These tasks are error-prone, in particular when they require copy-and-pasting data in e. g. spreadsheets. Also, a clear and unified documentation of the applied constants and the way of saving data is desirable. Additionally, the statistical methods, for example for outlier correction, should undergo clear documentation. Altogether, this helps to report Th/U ages in a standardized way (Dutton et al., 2017).

In this study, we present our user-friendly GUI and the underlying algorithm for data treatment and age calculation. The software is currently optimized for ThermoFisher Neptune MC-ICP-MS instruments, but the open-source code in principle allows adaptations to other setups and instruments. Methods to treat outliers in measurement data are particularly highlighted. As a case study, we present newly obtained ages from a stalagmite from Larga Cave, Puerto Rico, which shows a modern growth phase, as well as continuous deposition during the last Glacial into the deglaciation, thus demonstrating the performance of our method for both very young and older sample materials. Our protocol enables a precise determination of speleothem growth rates, which allows a comparison to a coevally deposited stalagmite from the same cave highlighting the influence of in-cave processes on speleothem growth rates. In particular, this dataset showcases how initial ^{230}Th correction models can be easily tested with our here presented software and GUI, and how those influence speleothem chronologies.

2 Methods

2.1 Standards and reference materials

We use our in-house triple spike solution (TriSpike) with a ^{233}U concentration of (0.038556 ± 0.0000009) ng/g, a ^{236}U concentration of (3.86778 ± 0.00009) ng/g and a ^{229}Th concentration of (0.018055 ± 0.000008) ng/g (2 standard error of the mean) (Kerber et al., 2023). For standard bracketing, we employ the Harwell-Uraninite 1 (HU-1) as a reference material. Its activity ratios ($^{230}Th/^{238}U$) and ($^{234}U/^{238}U$) are presumed to be 1, as it is a secular equilibrium material. Abundance sensitivity and hydride correction are determined by measuring CRM-112A U reference solution and an in-house ^{232}Th standard. The CRM-112A gravimetric standard solution has a ^{238}U concentration of (4.3021 ± 0.0015) µg/g, while the inhouse ^{232}Th standard calibrated with TriSpike has a ^{232}Th concentration of (505.8 ± 1.02) ng/g (2 σ uncertainties). CRM-112A solution is also used to track the values of the two ghost signal constants, k_{229} and k_{230} (Kerber et al., 2023). For k_{229}, it is measured without addition of TriSpike, while in the case of k_{230}, the spiked CRM-112A solution is employed. For age determination, the ^{230}Th and ^{234}U decay constants determined by Cheng et al. (2013) are used. Ages are reported with 2 σ statistical standard mean error, but do not include half-life uncertainties.

2.2 Chemical preparation and instrumentation

The chemical preparation of carbonate samples includes sample dissolution in ultra clean nitric acid, spiking with TriSpike and two steps of wet column chromatographic ion exchange separation of U and Th from matrix elements using Eichrom UTEVA resin (Douville et al., 2010; Wefing et al., 2017; Matos et al., 2015). Chemical blanks are commonly below 0.4 fg for ^{234}U and 0.04 fg for ^{230}Th and Ca matrix concentrations are required to be below 10 ppm. For the mass-spectrometric measurement, samples are dissolved in 1 % HNO_3 and 0.05 % HF. All samples were measured on a MC-ICP-MS (ThermoFisher Neptune Plus) at the Institute for Environmental Physics, Heidelberg University (Germany). The desolvating system CETAC Aridus II is used as inlet.

The mass spectrometer is equipped with Faraday cups (FC) and a central secondary electron multiplier (SEM). The central detector can be selected between the SEM and a FC connected to a 10^{13} Ω amplifier. ^{238}U is measured on a 10^{10} Ω amplified resistor. All other FC are connected to 10^{11} Ω amplifiers. The cup setting to collect isotope signals on masses 238 to 229 is shown in table 2 in Kerber et al. (2023). The first cycle collects all U isotopes for 2 seconds, with ^{234}U on the central detector (FC/SEM). The second and third cycle collect the Th isotopes for 2

seconds integrations time, with ^{230}Th and ^{229}Th on the central SEM. These cycles are repeated for an optimal number for each measurement.

A measurement sequence starts with the determination of abundance sensitivity and tailing on two different solutions for both uranium and thorium. Each sample and standard measurement is preceded by a procedural blank measurement to ensure that the background signal has gone back to a clean state. CRM-112A measurements are carried out to track ghost signal values at the beginning and end of a measurement sequence. Samples are bracketed with HU-1 as a reference material. Samples, standard, and procedural blanks are measured with the same configuration.

Mass fractionation (or mass bias) is corrected via the natural ratio of $^{235}U/^{238}U$ due to the lack of natural Th isotopes. In our setup, the ratio of the artificial isotopes $^{233}U/^{236}U$ ratio in the spike is monitored for double checking the mass bias correction. The calibration of FC gain and SEM yield is described in detail in Kerber et al., (2023): While there is an internal electronic calibration function for the calibration of 10^{10} Ω and 10^{11} Ω amplifiers, the 10^{13} Ω amplifier in our setup is calibrated manually. For this, the gain factor is determined regularly by measuring ^{235}U alternately on the 10^{13} Ω and 10^{11} Ω amplified cup. In an analogous manner, the SEM yield is routinely determined by measuring ^{235}U alternating on the SEM and on a 10^{11} Ω FC at a signal intensity of ~ 5 mV. Since HU-1 standards are measured with the same detector configuration in standard bracketing mode, the observation of the ($^{234}U/^{238}U$) values of HU-1 measurements allows monitoring and manual optimization of gain and yield values for each measurement sequence in the data analysis scheme.

In its current version, the GUI is written for this type of measurement protocol. Many adaptions, such as fewer procedural blank measurements, other isotope ratios for mass fractionation correction or similar require small changes in the code, but are easily feasible for users sufficiently competent in Python. Numerous MC-ICP-MS instruments, measurement protocols, and cup configuration settings can be used for such isotope measurements.

Here, we have developed our data treatment and GUI for a quasi-simultaneous measurement of U and Th isotopes as detailed previously (Kerber et al., 2023). We do not need to specify the number of cycles or the exact scheme of the sequence as the software will extract this information from the data. However, the cup configuration matters. Our method implies that U and Th isotopes are present in the final solutions, which requires a U isotope scattering correction. This is not necessarily needed when measuring U and Th isotope solutions independently. Nevertheless, the here presented open-source software can easily be adopted to other cup configurations or raw data outputs from different instruments.

2.3 Speleothem sample description

Stalagmite B1 was collected in 2019 in Larga cave, Puerto Rico (18°19′N 66°48′W, 350msl, supplementary Figure S1A) from a passage in the deep part of the cave connected to the “Collapse room”. The host rock overburden at the location of the sample is about 40-60m. It is in total 60 cm long, and has an average diameter of 15 cm (supplementary Figure S1B). The drip site was still active, and was monitored with spot measurements over several years, revealing varying drip intervals between 2 s and >120 s. A total amount of 37.7 ml water from the drip site of stalagmite B1 was analysed for its U and Th activity ratios. Samples for ^{230}Th/U dating of the speleothem with typical input masses of 100-150 mg have been cut using a diamond wire saw along the growth axis. Chemical preparation, mass-spectrometric measurements, data treatment and evaluation of drip water and the speleothem samples followed the methods described in Kerber et al. (2023) and in this study.

Larga Cave is located in the north central karst region of Puerto Rico (supplementary Figure S1A). Previous work including extensive cave air and drip monitoring has demonstrated that the cave is a valuable location to study of the influence of changing climate on past rainfall patterns in the Western tropical Atlantic (Vieten et al., 2018a; Warken et al., 2022b; Vieten et al., 2018b). In particular, the main passage of Larga Cave is subject to a seasonally varying ventilation, which results in pCO_2 values of 600 ppm close to atmospheric values during winter, and higher values up to 1800 ppm in summer (Vieten et al., 2016). In contrast, in the deep part of the cave, where also stalagmite B1 was collected, ventilation is strongly muted, and cave air pCO_2 values are higher with values up to 2300 – 3600 ppm (Vieten et al., 2016). As a result of this ventilation regime, growth rates are expected to vary both seasonally, but also between different locations inside the cave (Vieten and Hernandez, 2021). So far, two speleothem records from Larga Cave are been published, where the most recent covers the past 500 years (Vieten et al., 2024), and the second stalagmite grew during the period of 46.2-15.3 ka with a hiatus from 41.1 to 35.5 ka (Warken et al., 2020). For ^{230}Th/U dating of Larga speleothems, high initial Th contents have to be considered - a phenomenon that regularly occurs in speleothem records from the Caribbean and Central American region (Fensterer et al., 2010; Steidle et al., 2021; Moseley et al., 2015; Schorndorf et al., 2023; Stinnesbeck et al., 2020; Beck et al., 2001; Akers et al., 2016; Rivera-Collazo et al., 2015).

3 Data treatment and analysis procedures

The whole analysis procedure from raw data treatment to age calculation is conducted in one GUI featuring three tabs: 'Input' for isotopic ratio calculations, 'Inspect' for outlier correction of the signal and 'Analysis' for age calculation. The source code is accessible at https://github.com/puahd/UTh_Analysis. It is based on the open source PyQt5 Python library (https://pypi.org/project/PyQt5/). To execute the GUI, the user has to run the file "main.py". The folder https://github.com/puahd/UTh_Analysis/dist also contains a compiled .exe file for the GUI ("UTh Data Analysis.exe") as well as default configuration files ("constants – coral.cfg" and "constants – stalag.cfg". Input and output format of files are .csv or .xlsx. The GUI consists of three consecutive tabs, for which the functionalities and the underlying calculations and processes will be described in the following.

3.1 Input tab

In 'Input', as presented in Figure 1, the user can navigate to the folder containing the raw mass spectrometer data and start the calculation of corrected isotopic ratios (Box 1 in Figure 1). All tab screenshots present data from stalagmite B1. Prior to the calculations, a configuration file containing all necessary constants used in the calculations needs to be loaded (same Box 1). This file contains constants and correction factors used for evaluation of the activity ratios and ages, such as mass fractionation coefficients, decay constants, the exact masses of the isotopes and the values applied for initial ^{230}Th correction model. All constants can be edited manually either in the configuration file directly, or within the GUI using the button "edit". An exemplary configuration table is also provided in the supplementary material (Figure S2). To apply a ^{230}Th correction model a value can be set for the activity ratio and uncertainty of the contaminating material ("A230Th232Th Init."). The conventional approach to account for initial Th would be an activity ratio of 0.75 ± 0.38, assuming an upper continental crust ^{232}Th/^{238}U weight ratio of 3.8 (Taylor and Mclennan, 1985) with an uncertainty of 50% (Ludwig and Paces, 2002) and ^{230}Th, ^{234}U, and ^{238}U in secular equilibrium for the detrital material. Exemplary templates for corals and speleothems with conventionally used correction models are provided. For speleothems, a typical

activity ratio of $(^{230}Th/^{232}Th)_{ini/detr}$ of detritus is estimated to 0.75 ± 0.38 (see above). Nevertheless, this ratio may require adjustment according to local conditions. The coral template assumes as default value an activity ratio of 8 ± 4, which is estimated for corals dwelling in waters of the northeast Atlantic upper thermocline (Wefing et al., 2017). For one data series, only one correction constant, the $(^{230}Th/^{232}Th)$ activity ratio of the contamination, can be added to the calculation. Hence, in case several factors need to be explored, the data series requires repeated treatment.

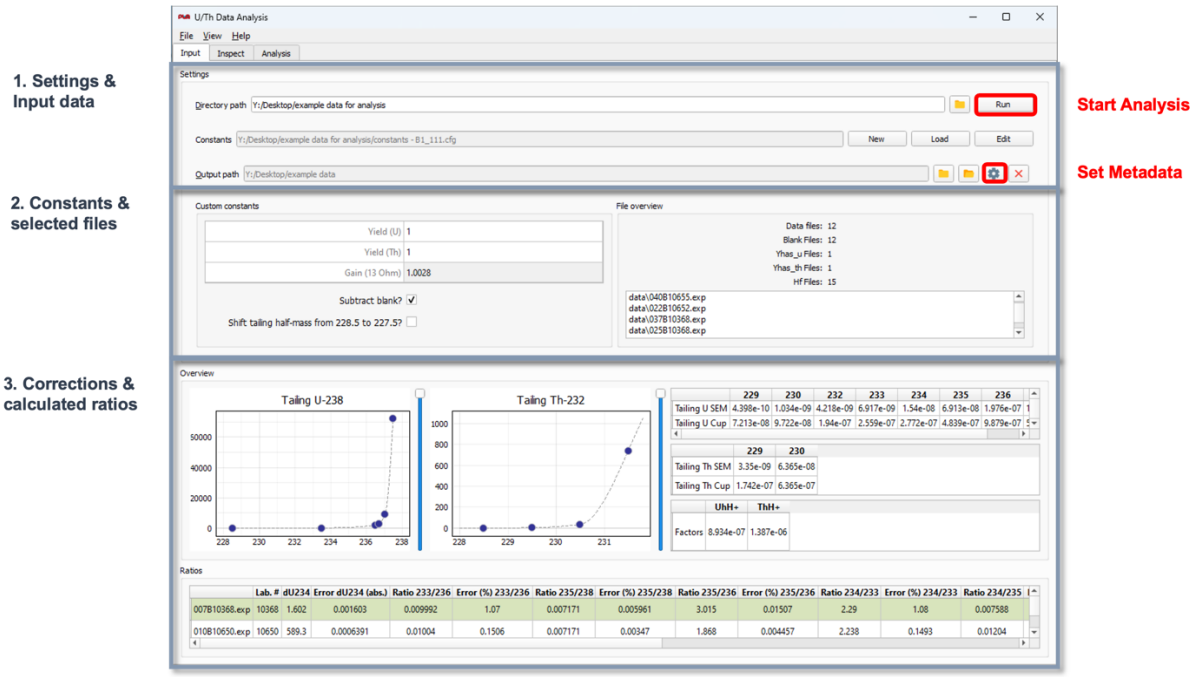

Figure 1. *Input tab: (1) In the top part the data folder is selected ("directory path"), the constants file ("constants") can be loaded ("load"), edited ("edit"), or created ("new"). In addition, it is possible to set an "output path". Red boxes show the "settings" button to enter metadata for saving, as well as the "run" button to start the analysis. Box (2) shows the custom constants box as well as the file overview for the selected folder. In box (3), the plots on the top left show the interpolated tailing. On the top right, numerical values of U and Th tailing and hydride correction are presented. The calculated ratios are shown in the bottom panel.*

Figure 1 shows the layout of the GUI 'Input' tab. Once the constants are implemented and the input data are selected, it is optional to choose an output path to store the analysis output (Box 1). If no path is specified, the results will be stored in the raw data folder. When clicking the settings button next to the output path (highlighted in red in Box 1), a menu opens in which the following parameters about the sample can be noted: denomination, type of archive, lab numbers, geographic origin, and a general description. The first and last laboratory number are automatically read out from the raw data. The final output result files will then be saved in a newly created folder under the name _[labnumber$_1$-labnumber$_n$] denomination in the directory chosen before. The metadata information transferred through the GUI dialogue window is stored in a .json file in the respective folder. In the 'custom constants' panel (Box 2), some settings can be selected, for example, if the blank has already been subtracted in the mass spectrometric software or not. Next to this panel, an overview over the files read in from the folder is shown. After running the evaluation script with the loaded data and adjusted settings (Button "run", highlighted in red in Box 1), the results of tailing and hydride correction, respectively as well as the calculated ratios are displayed in the tab (Box 3). In addition, four excel .xlsx output files are created by the software at this stage and stored in the directory path folder: Ratios.xlsx, Tailing.xlsx, PrBlank.xlsx and Intensities.xlsx.

Ratios.xlsx contains all calculated ratios and their errors as also presented in the GUI (Box 3). Tailing.xlsx summarizes the U and Th tailing values (in cps/V ^{238}U) for each mass. In PrBlank.xlsx, the average values for each mass of the procedural blank measurements before each standard and sample are presented. Intensities.xlsx contains the full data tables, with the signals in cps or V for each mass over all cycles. Every standard or sample has its own sheet.

The algorithm of the 'Input' tab starts by reading in the '.exp' measurement files for sample and standard measurements, process blank (=instrumental background) and Uranium and Thorium abundance sensitivity measurements. The lines for all cycles for all isotopes are imported into a pandas data frame. Firstly, matrices for tailing, hydride and process blank correction are produced that are later subtracted from the isotopic masses used for ratio building. The individual steps are carried out as follows:

- Tailing: Uranium tailing is determined by measuring the off-masses 228.5, 233.5, 236.5, 236.7, 237.05 and 237.5 before a measurement sequence starts. The first half-mass can be changed between 228.5 and 227.5 as we observed a scatter peak around this mass that switched its exact position every few months. Thorium tailing off-masses are 227.5, 228.5, 229.5, 230.5 and 231.5. For interpolation to full masses, we use piecewise cubic Hermite interpolating polynomial fits (Kerber et al. 2023). The masses that undergo ^{238}U tailing correction are ^{233}U, ^{234}U, ^{235}U, ^{236}U, ^{229}Th, ^{230}Th and ^{232}Th, while ^{232}Th correction is applied to ^{229}Th and ^{230}Th.
- Hydride isobaric interference: Hydride correction is determined by measuring 239 amu for UH^+ and 233 amu for ThH^+ during the abundance sensitivity measurements. The instrumental background (or memory) is here referred to as process blank. It is measured between all sample and standard measurements for 70 s. Typical blank levels afterwards are 0.5 cps for ^{230}Th and 6 cps for ^{234}U. The matrices from these three corrections are then used for data reduction of each isotope.
- Detector setting: Three main different detector layouts are possible and are detected automatically by the software: 1) all isotopes on cup, 2) ^{234}U, ^{230}Th and ^{229}Th on SEM and 3) ^{234}U on FC, ^{230}Th and ^{229}Th on SEM. In normal operation, option 2) and 3) are used, depending on the ^{234}U concentration of the respective samples. ^{234}U signals above 2 mV are measured on the center FC which is the case for the absolute majority of samples.

The sample and standard data are corrected for yield, gain and mass fractionation, are now used for the calculation of all relevant isotopic ratios followed by subsequent outlier tests, as described in Section 3.2.

3.2 Inspect Tab

Following the initial raw data treatment in the Input Tab, the 'Inspect' tab (presented in Figure 2) allows to visualize and retreat the data prior to final age calculation. In particular, the settings for the outlier test can be adapted.

The Inspect tab allows the user to plot the signal datapoints over the measurement cycle number for all isotopes in the individual measurement files of the sequence. In the top of the tab (1), the ratio results table from the 'Input' tab is presented. On the left (2), the list of measurement files (.exp) is shown. By clicking on a specific file, the metadata and the signal plotted over the measurement cycle number are presented (3). On the bottom left (4), four dropdown menus are available: The first one, "Isotope", allows to select one isotope from all of the isotope species

measured. “Mean” offers to switch between mean and median of the signal. The “Deviation” menu provides three options for the assessment of data dispersion: standard deviation, median absolute deviation and interquartile range. By setting “Scaling” to absolute or relative, the y-axis of the plot on the right can be changed between signal intensities in V or cps and relative values. Any selection in the dropdown menus leads to an automatic update of the plot on the right. Mean resp. median, as well as the dispersion ranges are presented as blue dashed lines. Data points outside of the dispersion range are marked in red as outliers.

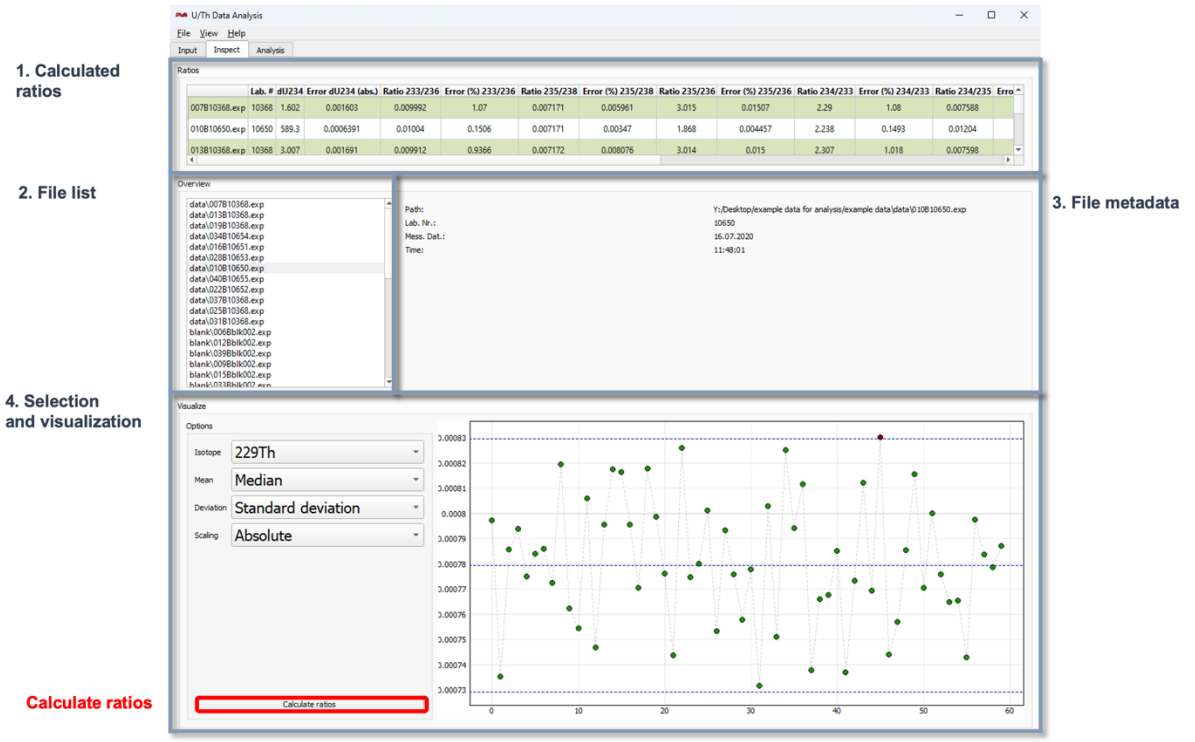

Figure 2: *Inspect tab. (1) Ratio results table (from Input tab), (2) Overview of measurement files in folder, (3) metadata of a selected file and signal over measurement cycle number for one isotope (which can be selected in (4)), (4) option selection panel for the signal plotting.*

The "Calculate ratios" button provides the option to recalculate the ratios using the updated mean and deviation selection for all isotopes. The default settings are median and standard deviation. However, these updated options are then used to exclude outliers from the ratio arrays, not the signal intensity arrays themselves. This means that not necessarily exactly the same data points are marked as outliers in the signal intensity plots and will be excluded, but the ones where signal ratios of two isotopes are outside of the accepted deviation range. The option selected in "Mean" will then also be used to calculate the average of the isotope ratios. The method of calculating the uncertainty of outlier-corrected isotopic ratios via the standard error, however, is fixed. In total, the software provides three different options for dispersion, including (i) the standard deviation (s), (ii) the interquartile range (IQR) (Tukey, 1977), and (iii) the median absolute deviation (MAD) (Leys et al., 2013; Huber, 2004; Rousseeuw and Croux, 1993). For the calculation of the MAD we assume normal distributed data. The treatment of means of ratios may have undesirable statistical properties for low or fast changing signals (Ogliore et al., 2011; Mclean et al., 2016), which could be taken into consideration when updating the software.

3.3 Analysis tab

In a last step, age calculation is carried out in the 'Analysis' tab presented in Figure 3. Here, additional input data is necessary from the sample weight tables (1). There are several ways to import these tables: Either by clicking "Load" and navigating to the respective folder, or by manually creating the table directly in the GUI ("Create"). An exemplary weight table is provided in the supplementary data (Figure 1). In the panel "Metadata history", the previously loaded sample weight tables in the directory path folder are shown, and can be directly imported. "Start Analysis" starts the data analysis and calculates the ages . Outputs are both presented in the GUI as result table and stored in an Results.xlsx file. In case an output path was specified, Results.xlsx is created both in the output and in the directory path folder. If the output path is missing, the file is only saved in the directory path folder. If an output directory has been created for specific lab numbers, all following analysis of these same files will be written to the same output directory, but not overwrite earlier Results.xlsx. The Results.xlsx has five sheets: *Inputs, Calc, Results, Constants* and *Options*. *Inputs* presents sample weight and metadata as well as the calculated ratios. In *Calc*, all steps of the age calculation such as concentrations and activity ratios are shown. *Results* is a summary of the most important calculation steps and final age values and the same table as is presented in the GUI as the results table in figure 3. *Constants* contains the whole list of values from the (potentially edited) '.cfg' file. In *Options* the average and dispersion measure option are stored.

The equations for activity ratios to calculate ages are implemented according to Ivanovich and Harmon (1992), with:

$$\left(\frac{^{234}U}{^{238}U}\right)(t) = \left(\left(\frac{^{234}U}{^{238}U}\right)_{init} - 1\right) \cdot e^{-\lambda_{234} \cdot t} + 1 \tag{4}$$

$$\left(\frac{^{230}Th}{^{238}U}\right) = 1 - e^{-\lambda_{230} t} + \frac{\delta^{234}U}{1000} \cdot \left(\frac{\lambda_{230}}{\lambda_{230} - \lambda_{234}}\right) \cdot \left(1 - e^{-(\lambda_{230} - \lambda_{234}) t}\right) \tag{5}$$

with

$$\delta^{234}U = \left(\left(\frac{^{234}U}{^{238}U}\right)_{meas} - 1\right) \cdot 1000\ (‰) \tag{6}$$

To obtain ages corrected for initial/detrital ^{230}Th, the $^{230}Th/^{238}U$ activity ratio used in eq. 5 is corrected using the initial $(^{230}Th/^{232}Th)_{ini/detr}$ ratio and

$$\left(\frac{^{230}Th}{^{238}U}\right)_{corr} = \left(\frac{^{230}Th}{^{238}U}\right)_{meas} - \left(\frac{^{232}Th}{^{238}U}\right)_{meas} \cdot \left(\frac{^{230}Th}{^{232}Th}\right)_{ini/detr} \left(\frac{\lambda_{230}}{\lambda_{230}-\lambda_{234}}\right) \cdot e^{-\lambda_{230} \cdot t} \quad (7)$$

These equations need to be solved numerically. For the determination of age uncertainty, the usual approach is to repeat the numerical determination of the age for several thousand runs in a Monte-Carlo simulation while random sampling the input ratios from a normal distribution with μ corresponding to the ratio's value and σ corresponding to the uncertainty on this parameter.

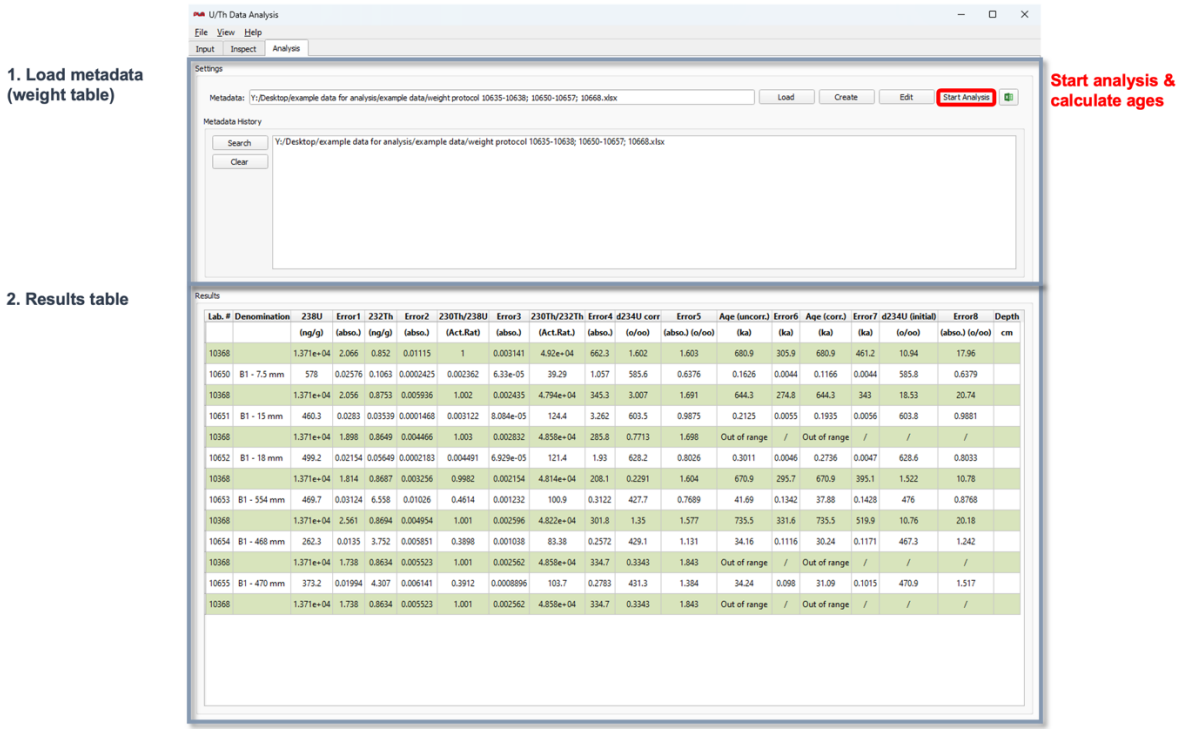

Lab. #	Denomination	238U	Error1	232Th	Error2	230Th/238U	Error3	230Th/232Th	Error4	d234U corr	Error5	Age (uncorr.)	Error6	Age (corr.)	Error7	d234U (initial)	Error8	Depth
		(ng/g)	(abso.)	(ng/g)	(abso.)	(Act.Rat)	(abso.)	(Act.Rat.)	(abso.)	(o/oo)	(abso.) (o/oo)	(ka)	(ka)	(ka)	(ka)	(o/oo)	(abso.) (o/oo)	cm
10368		1.371e+04	2.066	0.852	0.01115	1	0.003141	4.92e+04	662.3	1.602	1.603	680.9	305.9	680.9	461.2	10.94	17.96	
10650	B1 - 7.5 mm	578	0.02576	0.1063	0.0002425	0.002362	6.33e-05	39.29	1.057	585.6	0.6376	0.1626	0.0044	0.1166	0.0044	585.8	0.6379	
10368		1.371e+04	2.056	0.8753	0.005936	1.002	0.002435	4.794e+04	345.3	3.007	1.691	644.3	274.8	644.3	343	18.53	20.74	
10651	B1 - 15 mm	460.3	0.0283	0.03539	0.0001468	0.003122	8.084e-05	124.4	3.262	603.5	0.9875	0.2125	0.0055	0.1935	0.0056	603.8	0.9881	
10368		1.371e+04	1.898	0.8649	0.004466	1.003	0.002832	4.858e+04	285.8	0.7713	1.698	Out of range	/	Out of range	/	/	/	
10652	B1 - 18 mm	499.2	0.02154	0.05649	0.0002183	0.004491	6.929e-05	121.4	1.93	628.2	0.8026	0.3011	0.0046	0.2736	0.0047	628.6	0.8033	
10368		1.371e+04	1.814	0.8687	0.003256	0.9982	0.002154	4.814e+04	208.1	0.2291	1.604	670.9	295.7	670.9	395.1	1.522	10.78	
10653	B1 - 554 mm	469.7	0.03124	6.558	0.01026	0.4614	0.001232	100.9	0.3122	427.7	0.7689	41.69	0.1342	37.88	0.1428	476	0.8768	
10368		1.371e+04	2.561	0.8694	0.004954	1.001	0.002596	4.822e+04	301.8	1.35	1.577	735.5	331.6	735.5	519.9	10.76	20.18	
10654	B1 - 468 mm	262.3	0.0135	3.752	0.005851	0.3898	0.001038	83.38	0.2572	429.1	1.131	34.16	0.1116	30.24	0.1171	467.3	1.242	
10368		1.371e+04	1.738	0.8634	0.005523	1.001	0.002562	4.858e+04	334.7	0.3343	1.843	Out of range	/	Out of range	/	/	/	
10655	B1 - 470 mm	373.2	0.01994	4.307	0.006141	0.3912	0.0008896	103.7	0.2783	431.3	1.384	34.24	0.098	31.09	0.1015	470.9	1.517	
10368		1.371e+04	1.738	0.8634	0.005523	1.001	0.002562	4.858e+04	334.7	0.3343	1.843	Out of range	/	Out of range	/	/	/	

Figure 3: *Analysis tab. (1) Load sample weight tables (metadata files). The bottom panel lists the history of previously loaded tables. The button highlighted in red starts the analysis to calculate ages ("Start Analysis") button. The panel in box (2) displays the results table.*

4 Example dataset: Stalagmite B1

To demonstrate our data evaluation tool, we here present newly obtained ages of stalagmite B1 from Larga Cave, Puerto Rico. The results of activity ratios and calculated ages can be accessed in the supplementary table S1. Analysis of the speleothem samples reveals moderate U concentrations in the range between 300 and 600 ng/g, and minor detrital ^{232}Th contamination with (^{230}Th/^{232}Th) activity ratios of typically >300. However, in both the top 20 mm and around 450 mm distance from top (dft) lower (^{230}Th/^{232}Th) activity ratios of c. 40 – 125 are measured. U isotopic composition varies between 450 and 640 ‰ of δ^{234}U values. Uncertainties of the uncorrected ages are typically in the range of 0.2 to 0.6 % (Table S1). Drip water shows high U concentration of 0.825 ng/g and elevated initial Th concentrations, with an activity ratio of K=(^{230}Th/^{232}Th)=11.1 ± 0.1. We have used the software to test how the chronology changes to assess the influence of a varying initial Th activity ratio. For this, we used three different correction models, including the measured initial Th ratio of the drip water (K=11.1 ± 0.1), the detrital correction value of K=0.75 ± 0.38 derived from the bulk Earth crust chemical composition, as well as a value of K=23.7 ± 7.5 as previously determined using isochrons on speleothem PR-LA-1 from the same cave (Warken et al. 2020). Figure S3 in the supplemental material shows the ages corrected for initial ^{230}Th using the three different models. Only the initial ^{230}Th value measured in the drip water yields a stratigraphic order of the corrected ages supporting the use of this value. Residual variability around the mean chronology increases and age inversions appear in the record when using a different value of K. Figure S4 shows different growth models for stalagmite PR-LA-B1. Growth rates vary between c. 10 and 150 µm/a, with highest values during the warm Bølling–Allerød period c. 13.97 ± 0.051 and 13.114 ± 0.073 ka BP as well as the late Holocene growth phase after 0.277 ± 0.008 ka BP. Lowest growth rates occur during the final stage of Heinrich Stadial (HS) 1 (16.23 ± 0.082 to 13.97 ± 0.051 ka BP), HS3 (31.02 ± 0.10 to 29.38 ± 0.12 ka BP), and HS4 (40.81 ± 0.16 to 39.12 ± 0.12 ka BP).

5 Discussion

5.1 Outlier correction

Outlier correction is carried out automatically by the software adapting the dispersion measure of the raw data and in the following we argue that generally means should be replaced by medians. Shao et al. (2019) had addressed this problem by implementing manual outlier removal by comparison to boxplots based on interquartile ranges. We opted for the automatic version as this is more time efficient for large datasets. The different dispersion measure options described in Section 3.2 are relevant because measurements are not always ideal cases with normally distributed data and thus outliers. During measurements, short-term system instabilities occur for a variety of reasons, such as varying gas flow in the inlet system, plasma instabilities, and varying size of sample aerosols causing outliers in the signal intensities. Even though only the ratios between the different isotopes are of interest, strong changes in signal intensity may lead to varying isotope ratios, as a result of changing variance. Such difference may be amplified by the use of different detectors or with respect to different magnetic field settings, which are not necessarily responding at exactly same amplitude. Moreover, signal decreases (detuning events and temporal clocking) cause the statistical variance to increase locally.

Figure 4 shows an example: The upper panel displays periodic dips in the ^{238}U signal intensity during a measurement. In the lower panel of Fig. 4, the uncorrected ($^{230}Th/^{238}U$) activity ratio for the same measurement is plotted. For both curves, the different measures to calculate dispersion are shown. It is clearly visible that the median agrees much better with the majority of signal intensity values than the mean, which is strongly influenced by the periodic dips due to the asymmetry in the statistical distribution. Such an obvious difference is not visible in the isotope ratio, but within the resulting uncertainty. Consequently, we propose to generally use the median instead of mean by default. This is more accurate in the case of asymmetric small-scale oscillations inside the non-outlier interval and has no disadvantages.

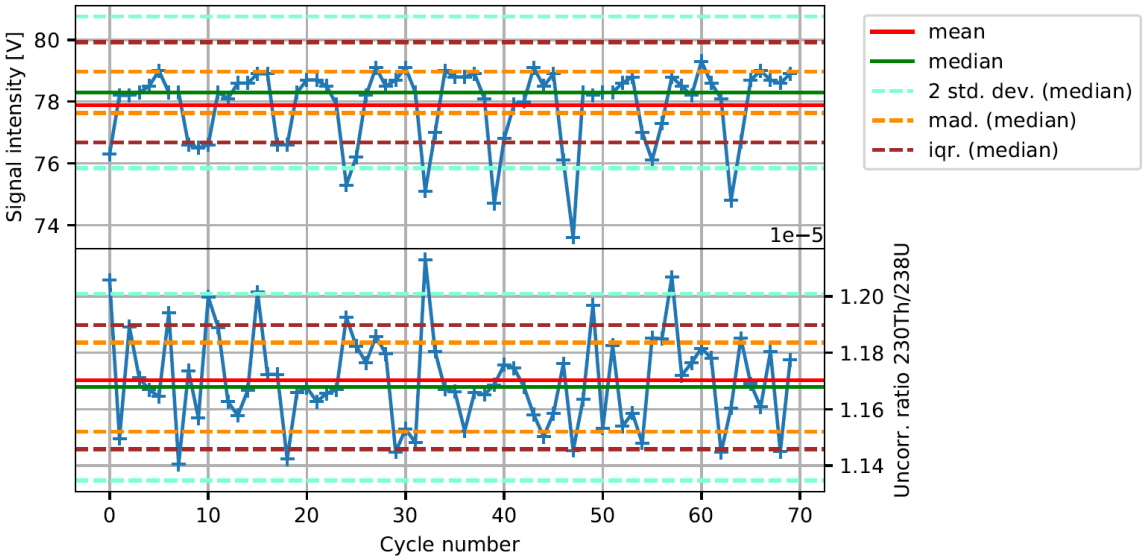

Figure 4: *Upper panel: ^{238}U signal intensities in Volt over measurement cycles for a carbonate sample during routine lab measurements. Lower panel: Corresponding uncorrected $^{230}Th/^{238}U$ ratio. Mean and median as well as the three different dispersion measures are plotted.*

Applying standard deviation as a dispersion measure in Figure 4 does not cover most of these outliers due to their large number and relatively small deviation. Thus, applying another dispersion measure for outlier removal is necessary here, and in addition more robust and easier to accomplish than manual deletion of all of the outliers. It is important, however, to stress that the outlier correction using the selected dispersion option is run on the calculated ratios after correction, not on the signal intensities themselves. This implies that when all isotopes are affected in the same way, they pass the outlier test. This is, however, unlikely at least for ratios of isotopes measured in different magnetic field settings. The dispersion measure of the outlier corrected ratio array is the same in every case, as described above.

5.2 Detrital thorium correction

Thorium correction is often crucial for studying carbonates where the correction is significant, but the initial ^{230}Th value is unknown, potentially variable, or when studying “dirty” carbonates such as tufa and travertine (Mallick and Frank, 2002; Hellstrom, 2006; Wenz et al., 2016). Several studies have shown that this correction is particularly important for speleothem records from the Caribbean and Central American region, where values where found including 2 ± 1 (Schorndorf et al., 2023) or 14 ± 4 (Moseley et al., 2015). In Larga Cave, initial ($^{230}Th/^{232}Th$) ratios are presumably even higher where (Warken et al., 2020) obtained a value of 23.7±7.5 using

isochrons on a stalagmite from the cave. Besides the terrestrial regime, this aspect is also relevant for marine archive such as corals, where studies propose a large range of seawater ($^{230}Th/^{232}Th$) activity ratios. While Cheng et al. (2000a) set the range to 80 ± 80 for deep-sea solitary corals, and Frank et al. (2004) calculated 10 ± 4 from seawater in the Eastern North Atlantic deep sea, values between 0.4 – 3.1 were determined for tropical corals (Shen et al., 2008). The range of both absolute values and uncertainties for these widely studied archives is hence enormous, and the choice of the appropriate correction model becomes particularly important, when (i) samples are very young and have generated only small amounts of ^{230}Th from U-decay, or (ii) when ultra-high precision is at play since any possible correction of the data contribute to the final age uncertainty. In our case study, we have run the correction of the ages of stalagmite B1 using three different correction models (Table S1). The resulting differences are visualized in Figure S3, and demonstrate the significant impact not only on absolute corrected ages, but also their uncertainties. For the young age at 7 mm dft (0.0466±0.0045 ka BP), the difference in the absolute corrected age when using another correction factor than the drip water value of K = 11.1±0.1 is c. ±50 years, which corresponds to a relative difference in the order of 100% (compare Table S1). Another example is the sample at 554 mm dft (37.81±0.14 ka BP for K=11.1±0.1), for which the other correction models also lead to substantially different ages of 41.37±0.19 ka BP (K=0.75±0.38) and 33.3±2.7 ka BP (K=23.7±7.5), hence the differences are still in the range of c. 10%. Notably, the low relative error of the initial ($^{230}Th/^{232}Th$) activity ratio of the drip water results in equally low uncertainties of the corrected age in the range of 0.4%. In contrast, the relative uncertainty of the age corrected with K=23.7±7.5 increases to 8%. Our GUI permits an easy adjustment of the initial ($^{230}Th/^{232}Th$) activity ratio for Th correction, which allows a direct assessment of the resulting corrected ages and uncertainties, and provides thus a convenient basis for further comparisons of the data. The use of a standardized software instead of handmade tuning reduces the susceptibility to potential errors, e.g., from copy-pasting, and ensures reproducibility in case a re-evaluation of the data is required to a later stage.

5.3 In-cave comparison of speleothem growth rates

The high number and precision of ^{230}Th/U ages of speleothem B1 allows investigation of growth rates changes. Comparison with northern hemispheric climatic changes suggests, that speleothem B1 growth is sensitive to prominent millennial-scale temperature variability, with higher growth rate during warmer phases and vice versa. In particular, during the cooler and drier Heinrich stadials (Warken et al., 2022a), growth rates are reduced. In addition, the results allow a comparison of the two coeval stalagmites from Larga Cave as shown in Figure S4. Overall, GRs of PR-LA-B1 are about 5 times lower than observed for PR-LA-1, where average annual growth rates are up to several mm/a. The difference in mean GR is also reflected in the shape of both speleothems, with PR-LA-1 exhibiting a large and variable diameter between c. 15 and 35 cm (Warken et al., 2020), while B1 is thinner with a diameter of 10-15 cm (supplementary Figure S1B). Differences in speleothem growth rates and the shape of a stalagmite may result from temperature, carbonate saturation, drip rate, and carbon dioxide contrast between cave air and saturation concentration of drip water (Merz et al., 2022; Skiba and Fohlmeister, 2023; Kaufmann, 2003; Dreybrodt, 1999). Ca concentrations in Larga Cave show no significant differences between drip sites (Vieten et al., 2018a, Vieten et al., 2018b, Warken et al., 2022). Therefore, the amplified GR and larger diameter of PR-LA-1 could be the result of the considerably lower pCO2 values in the main passage than compared to the back part of the cave (Vieten et al., 2016; Vieten and Hernandez, 2021), which facilitates enhanced oversaturation of the drip water with respect to calcite, and hence, stronger degassing of CO_2 and speleothem growth (Merz et al., 2022). Hence, the two stalagmites reveal growth differences potentially related to ventilation conditions.

6 Conclusion

We here provide an algorithm combined with a user-friendly GUI application for the treatment of ^{230}Th/U MC-ICP-MS data obtained by ThermoFisher Neptune instruments, and subsequent age calculation and correction. The two so far published programs explicitly aimed at ^{230}Th/U dating data reduction and age calculation are both written for ThermoFisher Neptune instruments as well. Pourmand et al. (2014) described a Mathematica routine, distributed as a Computable Document Format (.cdf) file, while Shao et al. (2019) had published a Matlab algorithm with GUI. We here have chosen to use Python for our algorithm and GUI to keep it open-source. The advanced user might want to change settings, which makes an opensource language and libraries a major advantage. However, the stand-alone executable .exe format of the GUI allows user-friendly handling also for non-programming experts. Our program supports multiple types of detector configurations: the FC-FC based approach as well as FC-SEM combining protocols. It is however adapted for combined Th and U measurements in three magnetic field lines (compare Kerber et al. (2023)), but other methods (such as separate solutions for Th and U) can be implemented with small changes in the code. Furthermore, we offer the first order Taylor derivation as a time-saving option for uncertainty calculation of final ages. Our application is especially designed to take reproducible and clear data management into account by a collection of methods: This includes that automatic creation of folders containing the results files and information on the sample metadata is possible and that .xlsx output files automatically contain all constants used for calculation, as well as the settings for outlier correction. Manually changing input constants, e. g. correction, of initial/detrital Th does not require to go to the code directly. So, the whole analysis scheme does not require any copy-and-pasting from one excel table to the other, and the constants used for calculation are easy to update.

Lastly, we demonstrated our protocols and data analysis scheme by accurately measuring and evaluating 30 speleothem ages from Larga Cave, Puerto Rico. Analyses of the growth rates and comparison with a coevally growing stalagmite from the same cave highlights the importance of in-cave processes for speleothem deposition rates.

Author contributions

IK - conceptualized the work, created and tested the implementation and operation of the code, co - supervised FK, who developed the code for the GUI and tested rigorously all corrections. NF - conceptualized the project, supervised IK, and FK and quality controlled the Th U isotope measurements of PR-LA-B1. SW - conceptualized the project, provided guidance on sample selection, verified the code and conceptualized the application. SW further evaluated the resulting age data on PR-LA-B1 and supervised a student project during which these and other data had been collected.

Code availability

The source code of "UTh Analysis" is accessible at https://github.com/puahd/UTh_Analysis. It is based on the open source PyQt5 Python library (https://pypi.org/project/PyQt5/). To execute the GUI, the user has to run the file "main.py". The folder https://github.com/puahd/UTh_Analysis/dist also contains a compiled .exe file for the GUI ("UTh Data Analysis.exe") as well as default configuration files ("constants – coral.cfg" and "constants – stalag.cfg". Example data for the analysis can be found in the supplementary material to this publication.

Data availability

Results of speleothem B1 ^{230}Th/U dating are available in the online supplementary material.

Sample availability

Sample material is available on request to swarken@iup.uni-heidelberg.de

Competing interests

At least one of the (co-)authors is a member of the editorial board of Geochronology.

Disclaimer

Acknowledgements

The authors are very thankful to the enormous support of the whole team of the research group „Physics of Environmental Archives" at Heidelberg University. Special thanks go to R. Eichstädter and A. Schröder-Ritzrau

for continuous engagement in the laboratory work and quality control. J. Arps is thanked for the development of a previous version of „UTh-Analysis". We are particularly grateful to R. Vieten for continuous support of speleothem research in Larga Cave. R. Vieten, N. Schorndorf, S. Therre and J. Förstel are thanked for their help in the field and with sample collection. We greatly acknowledge the work of N. Schorndorf, J. Schandl, and J. Gafriller on the chronology of speleothem B1. J. Bühler, C. Roesch, and K. Rehfeld are thanked for providing access and support with the age-depth modelling code. N. Frank received financial support for ^{230}Th/U measurements (DFG Grant N°256561558) and for the installation of the MC-ICPMS facility (DFG Grant N°247825108). S. Warken received financial support for the climate study of Puerto Rican speleothems via the DFG (Grant N° 512385350) and by Heidelberg University via the Olympia Morata program.

References

Akers, P. D., Brook, G. A., Railsback, L. B., Liang, F. Y., Iannone, G., Webster, J. W., Reeder, P. P., Cheng, H., and Edwards, R. L.: An extended and higher-resolution record of climate and land use from stalagmite MC01 from Macal Chasm, Belize, revealing connections between major dry events, overall climate variability, and Maya sociopolitical changes, Palaeogeography Palaeoclimatology Palaeoecology, 459, 268-288, 10.1016/j.palaeo.2016.07.007, 2016.

Akers, P. D., Brook, G. A., Railsback, L. B., Cherkinksy, A., Liang, F., Ebert, C. E., Hoggarth, J. A., Awe, J. J., Cheng, H., and Edwards, R. L.: Integrating U-Th, 14C, and 210Pb methods to produce a chronologically reliable isotope record for the Belize River Valley Maya from a low-uranium stalagmite, The Holocene, 29, 1234-1248, 10.1177/0959683619838047, 2019.

Andersen, M. B., Stirling, C. H., Potter, E. K., and Halliday, A. N.: Toward epsilon levels of measurement precision on 234U/238U by using MC-ICPMS, International Journal of Mass Spectrometry, 237, 107-118, 10.1016/j.ijms.2004.07.004, 2004.

Beck, J. W., Richards, D. A., Edwards, R. L., Silverman, B. W., Smart, P. L., Donahue, D. J., Hererra-Osterheld, S., Burr, G. S., Calsoyas, L., Jull, A. J., and Biddulph, D.: Extremely large variations of atmospheric 14C concentration during the last glacial period, Science, 292, 2453-2458, 10.1126/science.1056649, 2001.

Bourdon, B., Turner, S., Henderson, G. M., and Lundstrom, C. C.: Introduction to U-series Geochemistry, Reviews in Mineralogy and Geochemistry, 52, 1-21, 10.2113/0520001 %J Reviews in Mineralogy and Geochemistry, 2003.

Breton, T., Lloyd, N. S., Trinquier, A., Bouman, C., and Schwieters, J. B.: Improving Precision and Signal/Noise Ratios for MC-ICP-MS, Procedia Earth and Planetary Science, 13, 240-243, https://doi.org/10.1016/j.proeps.2015.07.056, 2015.

Cheng, H., Adkins, J., Edwards, R. L., and Boyle, E. A.: U-Th dating of deep-sea corals, Geochimica et Cosmochimica Acta, 64, 2401-2416, https://doi.org/10.1016/S0016-7037(99)00422-6, 2000a.

Cheng, H., Edwards, R. L., Hoff, J., Gallup, C. D., Richards, D. A., and Asmerom, Y.: The half-lives of uranium-234 and thorium-230, Chemical Geology, 169, 17-33, 10.1016/s0009-2541(99)00157-6, 2000b.

Cheng, H., Lawrence Edwards, R., Shen, C.-C., Polyak, V. J., Asmerom, Y., Woodhead, J., Hellstrom, J., Wang, Y., Kong, X., Spötl, C., Wang, X., and Calvin Alexander, E.: Improvements in 230Th dating, 230Th and 234U half-life values, and U–Th isotopic measurements by multi-collector inductively coupled plasma mass spectrometry, Earth and Planetary Science Letters, 371-372, 82-91, 10.1016/j.epsl.2013.04.006, 2013.

Chiang, H.-W., Lu, Y., Wang, X., Lin, K., and Liu, X.: Optimizing MC-ICP-MS with SEM protocols for determination of U and Th isotope ratios and 230Th ages in carbonates, Quaternary Geochronology, 50, 75-90, 10.1016/j.quageo.2018.10.003, 2019.

Douville, E., Sallé, E., Frank, N., Eisele, M., Pons-Branchu, E., and Ayrault, S.: Rapid and accurate U–Th dating of ancient carbonates using inductively coupled plasma-quadrupole mass spectrometry, Chemical Geology, 272, 1-11, 10.1016/j.chemgeo.2010.01.007, 2010.

Dreybrodt, W.: Chemical kinetics, speleothem growth and climate, Boreas, 28, 347-356, 1999.

Dutton, A., Rubin, K., McLean, N., Bowring, J., Bard, E., Edwards, R. L., Henderson, G. M., Reid, M. R., Richards, D. A., Sims, K. W. W., Walker, J. D., and Yokoyama, Y.: Data reporting standards for publication of U-series data for geochronology and timescale assessment in the earth sciences, Quaternary Geochronology, 39, 142-149, https://doi.org/10.1016/j.quageo.2017.03.001, 2017.

Fensterer, C., Scholz, D., Hoffmann, D., Mangini, A., and Pajón, J. M.: 230Th/U-dating of a late Holocene low uranium speleothem from Cuba, IOP Conference Series: Earth and Environmental Science, 9, 012015, 10.1088/1755-1315/9/1/012015, 2010.

Frank, N., Paterne, M., Ayliffe, L., van Weering, T., Henriet, J.-P., and Blamart, D.: Eastern North Atlantic deep-sea corals: tracing upper intermediate water Δ14C during the Holocene, Earth and Planetary Science Letters, 219, 297-309, 10.1016/s0012-821x(03)00721-0, 2004.

Hellstrom, J.: Rapid and accurate U/Th dating using parallel ion-counting multi-collector ICP-MS, Journal of Analytical Atomic Spectrometry, 18, 10.1039/b308781f, 2003.

Hellstrom, J.: U–Th dating of speleothems with high initial 230Th using stratigraphical constraint, Quaternary Geochronology, 1, 289-295, 2006.

Hoffmann, D. L., Prytulak, J., Richards, D. A., Elliott, T., Coath, C. D., Smart, P. L., and Scholz, D.: Procedures for accurate U and Th isotope measurements by high precision MC-ICPMS, International Journal of Mass Spectrometry, 264, 97-109, 10.1016/j.ijms.2007.03.020, 2007.

Huang, S., Cai, Y., Cheng, H., Xue, G., Cheng, X., He, M., Li, R., Ma, L., Wei, Y., Lu, Y., Yang, L., and Edwards, R. L.: An integrated study of constraining the initial 230Th of a stalagmite and its implications, Quaternary Geochronology, 80, 101497, https://doi.org/10.1016/j.quageo.2024.101497, 2024.

Huber, P. J.: Robust statistics, John Wiley & Sons2004.

Ivanovich, M. and Harmon, R.: Uranium series disequilibrium. Applications to environmental problems. Clarendon, 1992.

Kaufmann, G.: Stalagmite growth and palaeo-climate: the numerical perspective, Earth and Planetary Science Letters, 214, 251-266, 10.1016/s0012-821x(03)00369-8, 2003.

Kerber, I. K., Arps, J., Eichstädter, R., Kontor, F., Dornick, C., Schröder-Ritzrau, A., Babu, A., Warken, S., and Frank, N.: Simultaneous U and Th isotope measurements for U-series dating using MCICPMS, Nuclear Instruments and Methods in Physics Research Section B: Beam Interactions with Materials and Atoms, 539, 169-178, https://doi.org/10.1016/j.nimb.2023.04.003, 2023.

Leys, C., Ley, C., Klein, O., Bernard, P., and Licata, L.: Detecting outliers: Do not use standard deviation around the mean, use absolute deviation around the median, Journal of Experimental Social Psychology, 49, 764-766, https://doi.org/10.1016/j.jesp.2013.03.013, 2013.

Li, T.-Y., Wang, X., Chen, C.-J., Tan, M., and Wu, Y.: Testing the initial 230Th/232Th for “Known Age Carbonate” and its significance for 230Th dating and paleoclimate research, Quaternary International, 607, 113-119, 2022.

Ludwig, K. and Paces, J.: Uranium-series dating of pedogenic silica and carbonate, Crater Flat, Nevada, Geochimica et Cosmochimica Acta, 66, 487-506, 2002.

Ludwig, K. R. and Titterington, D. M.: Calculation of (230)Th/U Isochrons, Ages, and Errors, Geochimica Et Cosmochimica Acta, 58, 5031-5042, Doi 10.1016/0016-7037(94)90229-1, 1994.

552 Mallick, R. and Frank, N.: A new technique for precise uranium-series dating of travertine micro-
553 samples, Geochimica et Cosmochimica Acta, 66, 4261-4272, https://doi.org/10.1016/S0016-
554 7037(02)00999-7, 2002.

555 Matos, L., Mienis, F., Wienberg, C., Frank, N., Kwiatkowski, C., Groeneveld, J., Thil, F., Abrantes, F.,
556 Cunha, M. R., and Hebbeln, D.: Interglacial occurrence of cold-water corals off Cape Lookout (NW
557 Atlantic): First evidence of the Gulf Stream influence, Deep Sea Research Part I: Oceanographic
558 Research Papers, 105, 158-170, 10.1016/j.dsr.2015.09.003, 2015.

559 McLean, N. M., Bowring, J. F., and Gehrels, G.: Algorithms and software for U-Pb geochronology by
560 LA-ICPMS, Geochemistry, Geophysics, Geosystems, 17, 2480-2496,
561 https://doi.org/10.1002/2015GC006097, 2016.

562 Merz, N., Hubig, A., Kleinen, T., Therre, S., Kaufmann, G., and Frank, N.: How the climate shapes
563 stalagmites—A comparative study of model and speleothem at the Sofular Cave, Northern Turkey,
564 Frontiers in Earth Science, 10, 10.3389/feart.2022.969211, 2022.

565 Moseley, G. E., Richards, D. A., Smart, P. L., Standish, C. D., Hoffmann, D. L., ten Hove, H., and
566 Vinn, O.: Early–middle Holocene relative sea-level oscillation events recorded in a submerged
567 speleothem from the Yucatán Peninsula, Mexico, The Holocene, 25, 1511-1521, 2015.

568 Ogliore, R., Huss, G., and Nagashima, K.: Ratio estimation in SIMS analysis, Nuclear instruments and
569 methods in physics research section B: beam interactions with materials and atoms, 269, 1910-1918,
570 2011.

571 Pourmand, A., Tissot, F. L. H., Arienzo, M., and Sharifi, A.: Introducing a Comprehensive Data
572 Reduction and Uncertainty Propagation Algorithm for U-Th Geochronometry with Extraction
573 Chromatography and Isotope Dilution MC-ICP-MS, Geostandards and Geoanalytical Research, n/a-
574 n/a, 10.1111/j.1751-908X.2013.00266.x, 2014.

575 Rivera-Collazo, I., Winter, A., Scholz, D., Mangini, A., Miller, T., Kushnir, Y., and Black, D.: Human
576 adaptation strategies to abrupt climate change in Puerto Rico ca. 3.5 ka, The Holocene, 25, 627-640,
577 10.1177/0959683614565951, 2015.

578 Rousseeuw, P. J. and Croux, C.: Alternatives to the Median Absolute Deviation, Journal of the
579 American Statistical Association, 88, 1273-1283, 10.1080/01621459.1993.10476408, 1993.

580 Roy-Barman, M. and Pons-Branchu, E.: Improved U–Th dating of carbonates with high initial 230Th
581 using stratigraphical and coevality constraints, Quaternary Geochronology, 32, 29-39,
582 https://doi.org/10.1016/j.quageo.2015.12.002, 2016.

583 Schorndorf, N., Frank, N., Ritter, S. M., Warken, S. F., Scholz, C., Keppler, F., Scholz, D., Weber, M.,
584 Aviles Olguin, J., and Stinnesbeck, W.: Mid-to late Holocene sea-level rise recorded in Hells Bells
585 234U/238U ratio and geochemical composition, Scientific Reports, 13, 10011, 2023.

586 Shao, Q.-F., Li, C.-H., Huang, M.-J., Liao, Z.-B., Arps, J., Huang, C.-Y., Chou, Y.-C., and Kong, X.-
587 G.: Interactive programs of MC-ICPMS data processing for 230Th/U geochronology, Quaternary
588 Geochronology, 51, 43-52, 10.1016/j.quageo.2019.01.004, 2019.

589 Shen, C.-C., Lawrence Edwards, R., Cheng, H., Dorale, J. A., Thomas, R. B., Bradley Moran, S.,
590 Weinstein, S. E., and Edmonds, H. N.: Uranium and thorium isotopic and concentration measurements
591 by magnetic sector inductively coupled plasma mass spectrometry, Chemical Geology, 185, 165-178,
592 https://doi.org/10.1016/S0009-2541(01)00404-1, 2002.

593 Shen, C.-C., Wu, C.-C., Cheng, H., Lawrence Edwards, R., Hsieh, Y.-T., Gallet, S., Chang, C.-C., Li,
594 T.-Y., Lam, D. D., Kano, A., Hori, M., and Spötl, C.: High-precision and high-resolution carbonate
595 230Th dating by MC-ICP-MS with SEM protocols, Geochimica et Cosmochimica Acta, 99, 71-86,
596 10.1016/j.gca.2012.09.018, 2012.

597 Shen, C.-C., Li, K.-S., Sieh, K., Natawidjaja, D., Cheng, H., Wang, X., Edwards, R. L., Lam, D. D.,
598 Hsieh, Y.-T., Fan, T.-Y., Meltzner, A. J., Taylor, F. W., Quinn, T. M., Chiang, H.-W., and Kilbourne,
599 K. H.: Variation of initial 230Th/232Th and limits of high precision U–Th dating of shallow-water
600 corals, Geochimica et Cosmochimica Acta, 72, 4201-4223, 10.1016/j.gca.2008.06.011, 2008.

601 Skiba, V. and Fohlmeister, J.: Contemporaneously growing speleothems and their value to decipher in-
602 cave processes–A modelling approach, Geochimica et Cosmochimica Acta, 348, 381-396, 2023.

603 Steidle, S. D., Warken, S. F., Schorndorf, N., Förstel, J., Schröder-Ritzrau, A., Moseley, G. E., Spötl,
604 C., Aviles, J., Stinnesbeck, W., and Frank, N.: Reconstruction of Middle to Late Quaternary sea level
605 using submerged speleothems from the northeastern Yucatán Peninsula, Journal of Quaternary Science,
606 10.1002/jqs.3365, 2021.

607 Stinnesbeck, W., Rennie, S. R., Avilés Olguín, J., Stinnesbeck, S. R., Gonzalez, S., Frank, N., Warken,
608 S., Schorndorf, N., Krengel, T., and Velázquez Morlet, A.: New evidence for an early settlement of the
609 Yucatán Peninsula, Mexico: The Chan Hol 3 woman and her meaning for the Peopling of the Americas,
610 Plos one, 15, e0227984, 2020.

611 Taylor, S. R. and McLennan, S. M.: The continental crust: its composition and evolution, 1985.

612 Töchterle, P., Steidle, S. D., Edwards, R. L., Dublyansky, Y., Spötl, C., Li, X., Gunn, J., and Moseley,
613 G. E.: 230 Th⁄U isochron dating of cryogenic cave carbonates, Geochronology, 4, 617-627, 2022.

614 Tukey, J. W.: Exploratory data analysis, Reading, MA1977.

615 Vieten, R. and Hernandez, F.: StalGrowth—A Program to Estimate Speleothem Growth Rates and
616 Seasonal Growth Variations, Geosciences, 11, 187, 2021.

617 Vieten, R., Warken, S., Winter, A., Schröder-Ritzrau, A., Scholz, D., and Spötl, C.: Hurricane Impact
618 on Seepage Water in Larga Cave, Puerto Rico, Journal of Geophysical Research: Biogeosciences, 123,
619 879-888, 10.1002/2017jg004218, 2018a.

620 Vieten, R., Winter, A., Warken, S. F., Schröder-Ritzrau, A., Miller, T. E., and Scholz, D.: Seasonal
621 temperature variations controlling cave ventilation processes in Cueva Larga, Puerto Rico, International
622 Journal of Speleology, 45, 259-273, 10.5038/1827-806x.45.3.1983, 2016.

623 Vieten, R., Warken, S., Winter, A., Scholz, D., Miller, T., Spötl, C., and Schröder-Ritzrau, A.:
624 Monitoring of Cueva Larga, Puerto Rico—A First Step to Decode Speleothem Climate Records, in:
625 Karst Groundwater Contamination and Public Health, edited by: White, W. B., Herman, J. S., Herman,
626 E. K., and Rutigliano, M., Advances in Karst Science, Springer International Publishing, Cham, 319-
627 331, 10.1007/978-3-319-51070-5_36, 2018b.

628 Vieten, R., Warken, S. F., Zanchettin, D., Winter, A., Scholz, D., Black, D., Koltai, G., and Spötl, C.:
629 Northeastern Caribbean rainfall variability linked to solar and volcanic forcing, Paleoceanography and
630 Paleoclimatology, 39, e2023PA004720, 2024.

631 Warken, S. F., Vieten, R., Winter, A., Spötl, C., Miller, T. E., Jochum, K. P., Schröder-Ritzrau, A.,
632 Mangini, A., and Scholz, D.: Persistent Link Between Caribbean Precipitation and Atlantic Ocean
633 Circulation During the Last Glacial Revealed by a Speleothem Record From Puerto Rico,
634 Paleoceanography and Paleoclimatology, 35, 10.1029/2020pa003944, 2020.

635 Warken, S. F., Weißbach, T., Kluge, T., Vonhof, H., Scholz, D., Vieten, R., Schmidt, M., Winter, A.,
636 and Frank, N.: Last glacial millennial-scale hydro-climate and temperature changes in Puerto Rico
637 constrained by speleothem fluid inclusion δ18O and δ2H values, Clim. Past, 18, 167-181, 10.5194/cp-
638 18-167-2022, 2022a.

639 Warken, S. F., Kuchalski, L., Schröder-Ritzrau, A., Vieten, R., Schmidt, M., Höpker, S. N., Hartland,
640 A., Spötl, C., Scholz, D., and Frank, N.: The impact of seasonal and event-based infiltration on transition
641 metals (Cu, Ni, Co) in tropical cave drip water, Rapid Communications in Mass Spectrometry, 36,
642 e9278, https://doi.org/10.1002/rcm.9278, 2022b.

643 Wefing, A.-M., Arps, J., Blaser, P., Wienberg, C., Hebbeln, D., and Frank, N.: High precision U-series
644 dating of scleractinian cold-water corals using an automated chromatographic U and Th extraction,
645 Chemical Geology, 475, 140-148, 10.1016/j.chemgeo.2017.10.036, 2017.

646 Wenz, S., Scholz, D., Sürmelihindi, G., Passchier, C. W., Jochum, K. P., and Andreae, M. O.: 230Th/U-
647 dating of carbonate deposits from ancient aqueducts, Quaternary Geochronology, 32, 40-52, 2016.

648 Wortham, B. E., Banner, J. L., James, E. W., Edwards, R. L., and Loewy, S.: Application of cave
649 monitoring to constrain the value and source of detrital 230Th/232Th in speleothem calcite:
650 Implications for U-series geochronology of speleothems, Palaeogeography, Palaeoclimatology,
651 Palaeoecology, 596, 110978, https://doi.org/10.1016/j.palaeo.2022.110978, 2022.

652 Zhao, J.-x., Yu, K.-f., and Feng, Y.-x.: High-precision 238U–234U–230Th disequilibrium dating of the
653 recent past: a review, Quaternary Geochronology, 4, 423-433, 10.1016/j.quageo.2009.01.012, 2009.
654